Mechanics & Industry **26**, 7 (2025)

https://doi.org/10.1051/meca/2024037

Mechanics & Industry

Available online at:
www.mechanics-industry.org

ORIGINAL ARTICLE OPEN ACCESS

Empirical formulation for bead shape prediction in direct energy deposition

Gyeong-Yun Baek*

Department of Convergence Mechanical Engineering, Gwangju University, Gwangju, Republic of Korea

Received: 9 April 2024 / Accepted: 18 December 2024

Abstract. In the metal deposition process, the bead shape plays a critical role in determining the precision and mechanical properties of the final product. Therefore, prior to additive manufacturing, it is essential to determine an optimal bead shape. In this study, the representation of bead shape using an empirical formulation in direct energy deposition, a metal additive manufacturing process, was investigated. Experiments were conducted by depositing SUS316 powder on an AISI D2 substrate and systematically varying major process parameters such as laser power and powder feed rate to observe the resulting changes in bead shapes. The findings revealed that the bead shape changed linearly in response to variations in these process parameters. Through detailed analysis, the effects and interactions of process parameters on the bead shape were predicted, and an empirical formulation based on changes in the cross section of real beads was derived. Remarkably, using only information related to process conditions, the bead shape and area were accurately predicted. Comparison of the cross-sectional values of the actual bead shape and the empirical formulation showed a maximum difference of 0.0287 mm^2 and a minimum difference of 0.0002 mm^2 in all experiments. These results provide valuable insights for establishing basic data that can be used to create an empirical formulation for bead cross-sectional shape and single bead volume in the metal additive manufacturing process.

Keywords: Bead shape prediction / bead volume / direct energy deposition / empirical formulation / SUS316

1 Introduction

Directed energy deposition (DED) is a metal additive manufacturing process that involves local irradiation of a high-power laser beam on a metal surface to create a melt pool and form a deposition surface. This process allows for 3D metal modeling through continuous deposition along a path calculated from a CAD model. DED offers unique characteristics, such as the ability to use various metal powders and achieve minimal dilution and low distortion of the workpiece due to excellent metal bonding [1,2]. As a result, DED is capable of forming complex shapes, reducing process time and costs, and enabling user-customized manufacturing, as well as repair and remanufacturing, making it applicable to various industries including automobiles, aerospace, construction, medical care, and electrical and electronic products. In the DED process, major process parameters, such as laser power, powder feed rate, scanning speed, and gas feed rate, have a decisive interaction with the bead shape. The bead shape and melting behavior significantly affect the bonding force with the substrate, mechanical properties, and microstructure, and numerous research studies have been conducted in these areas [3].

For instance, Oliveira et al. investigated the correlations between process parameters and geometric characteristics of the bead in coaxial layer cladding [4]. Hwang et al. studied the effect of process parameters on the substrate and deposition in the DED method, observing that higher laser power and powder feed rate resulted in more even deposition and increased bead height, while higher scanning speed and gas feed rate led to decreased deposition height [5]. Shin et al. analyzed the effects of changes in laser power, powder feed rate, scanning speed, and gas feed rate on the base and deposition using STS304L powder, and established the most efficient deposition process while also examining the changes in tensile strength [6]. Kim et al. investigated the effects of welding parameters on bead shape in MIG overlay welding and derived optimal process conditions for multi-pass overlay welding [7]. Bi et al. explored the influence of process parameters on product dimensions and material properties, such as deposition thickness, fractures, and porosity ratio, and proposed strategies for improving microstructure, hardness homogeneity, and dimensional accuracy through

* e-mail: gybaek@gwangju.ac.kr

Table 1. Chemical composition of materials.

Materials used	Element (wt%)								
	C	Si	Mn	P	S	Ni	Cr	Mo	V
AISI D2	1.56	0.24	0.25	0.03	0.001	0.18	11.31	0.83	0.35
AISI SUS316	0.08	1	2	0.045	0.03	12	17	2.5	–

process parameter control [8]. Based on these experimental studies, researchers have recognized the importance of process conditions in additive manufacturing and have reported on process condition optimization to establish suitable conditions for manufacturing high-quality products. Therefore, the development of an empirical formulation for bead shape is essential to shorten processing time and achieve desired quality in shape manufacturing.

Numerous studies have been conducted to develop empirical formulations for optimizing the bead shape in welding, which shares similarities with the DED process. Kim et al. proposed an analytical approach for optimizing the process parameters of the GMA welding process [9]. Researchers are also investigating the development of mathematical models to predict the optimal bead shape by analyzing the influence of process parameters on the bead shape. For instance, Kim et al. developed an empirical formulation for bead shape based on process parameters such as bead height, width, and pitch, to automate the multi-pass overlay welding process [10]. Dey et al. analyzed the effects of electron beam-induced current, accelerating voltage, and welding speed on the bead in the overlay welding process to develop a mathematical model for predicting bead height, width, and penetration depth [11]. In the welding of nickel-based overlays deposited by plasma arc welding, Siva et al. analyzed the effects of welding current, vibration amplification, welding speed, preheating temperature, and powder feed rate on the bead to develop a mathematical model for predicting the bead dimensions [12]. Cheikh analyzed the effects of laser power, scanning speed, and powder feed rate on the bead height, bead width, and area in the DED process, and developed a mathematical model to predict the bead cross section and the bead track shape [13]. Davim developed and verified a mathematical model using multiple regression analysis for cladding geometry according to the process parameters in the powder laser cladding process [14]. However, most of the studies focus on the optimization of bead shape and rely on mathematical models that assign weights to process factors, which can be complex, time-intensive, and may introduce shape errors depending on the weight.

In this study, additive manufacturing of SUS316 material using the DED process was conducted, and a factor analysis based on the process parameters was performed to address the challenge of predicting bead geometry with high precision. The newly proposed mathematical model aims to accurately predict the cross-sectional shape and volume of a single bead, enhancing the efficiency of the design phase in metal additive manufacturing. After varying the process parameters and performing additive manufacturing, cross-sectional samples from the actual beads were obtained, and their height and width were measured. This approach allows for an analysis of the effects and weights of the process parameters on bead shape. The predictive model was validated by comparing the actual measured dimensions of the bead cross-sections. The cross-sectional dimensions model also enabled the calculation of the bead volume. As a result, the bead shape was successfully derived and the bead area was predicted using only the information related to the process conditions.

2 Materials and methods

2.1 Materials

Table 1 presents the chemical composition of the materials used in this study. The substrate material used was AISI D2, a commonly used cold alloy tool steel, which was fabricated through a rolling process. The deposition material selected was SUS316, a widely used austenitic stainless steel powder in DED due to its excellent high-temperature strength and corrosion resistance. The metal powder was stored in a humidity-controlled chamber, and to achieve a dense structure with reduced pores in the melting process, a powder with a diameter ranging from 50 to 150 μm was utilized (Fig. 1).

2.2 Experimental methods

The DMT MX3 (InssTek Int.) system was employed for the metal deposition process in this study. This system consists of a hopper, powder nozzle, and process gas feed system, where the laser beam and powder are simultaneously sprayed from the nozzle (Fig. 2). Among the various deposition process parameters, the laser power, powder feed rate, scanning speed, and gas feed rate are critical factors that impact the bead shape and bonding force with the substrate. Thus, these process parameters were selected, and 25 mm of SUS316 powder was deposited on the surface of the substrate ($50 \times 100 \times 10$ mm). The experimental conditions are listed in Table 2. Each of the three major process parameters, namely, laser power, powder feed rate, and scanning speed, were varied in Cases 1, 2, and 3 for deposition, each conducted in triplicate. Meanwhile, the coaxial gas (Ar) feed rate was kept fixed. To observe the changes in the shape of the deposited section corresponding to the variations in the major process parameters, the deposited bead was cut as shown in

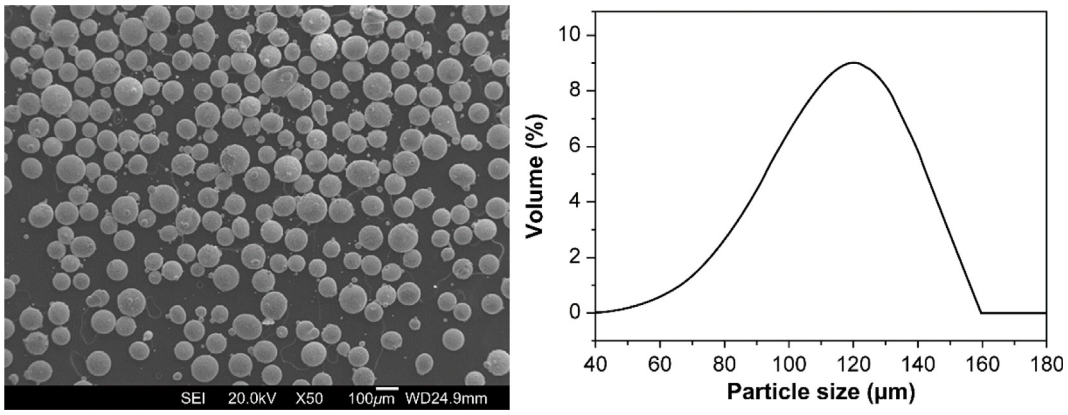

Fig. 1. SEM image and particle distribution of SUS316 powder.

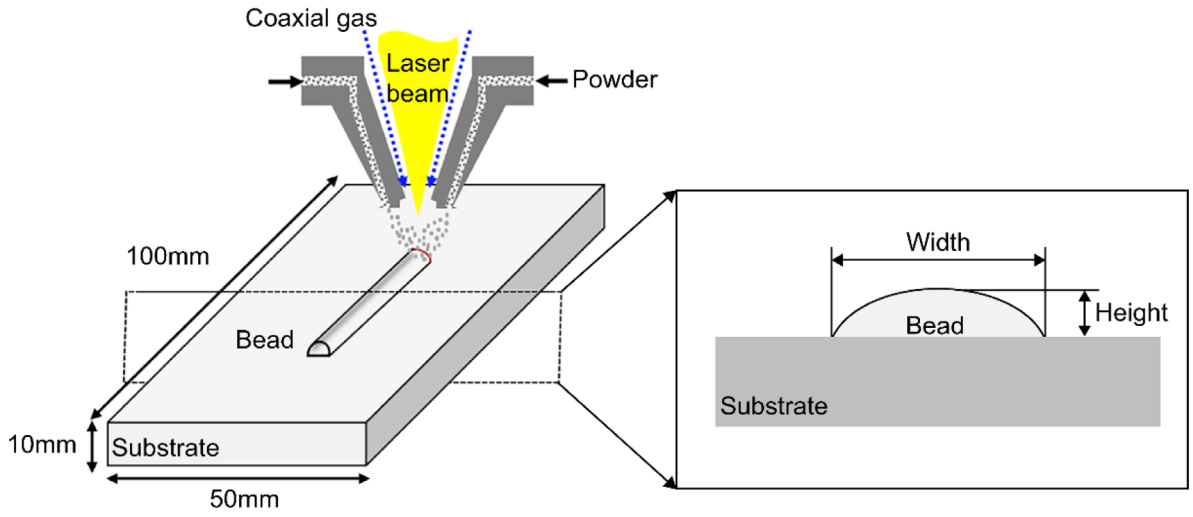

Fig. 2. Schematic of deposited bead.

Figure 2, and the width (W) and height (H) of the bead were measured in the cross section using an optical microscope.

2.3 Deriving empirical formulation

In accordance with the findings from the previous section, all deposited beads exhibited a consistent semicircular shape. To mathematically model this shape, a quadratic function was derived, as depicted in Figure 3. The general expression for a quadratic function is given by equation (1), and the coefficient of x in equation (1) can be obtained using equation (2). In this case, h and w represent the height and width of the bead cross section, respectively. In order to utilize the semicircular portion of the quadratic function as the bead shape, the coefficient a is set to a negative value. By setting the x axis of the graph as the bead width and y axis as the bead height, as it is a quadratic function graph passing through the three points $\left(-\frac{w}{2},0\right),\left(\frac{w}{2},0\right),(0,h)$, a graph was derived using the coefficient values $a=\frac{h}{-\frac{w}{2}\times\frac{w}{2}}=-\frac{4h}{w^2}, c=h$. Additionally, to deduce the height and width of the beads based on process variables, this study derived coefficients A, B, and C. Coefficient A, defined as $A=\mu\text{m/W}$, is used to convert laser power (W) into units of bead height or width (μm). Similarly, coefficient B, expressed as $B=\mu\text{m}\cdot\text{min/mm}$, applies to the conversion of scanning speed (mm/min), and coefficient C, $C=\mu\text{m}\cdot\text{min/g}$, is used for converting the powder feed rate (g/min). Using these coefficients, it is possible to translate the varied process settings into measurable dimensions of bead height or width. Furthermore, to assess the disparity in shape between the empirical formulation and the actual bead, the area of the cross-section of each bead was measured and compared, allowing for a direct comparison of theoretical predictions to actual outcomes.

$$y=ax^2+c \tag{1}$$

$$a=-\frac{4h}{w^2}, c=h. \tag{2}$$

Table 2. Processing parameters for DED used in this study.

Experiment	Laser power (W)	Powder feed rate (g/min)	Scanning speed (mm/min)	Coaxial gas (g/min)
Case 1	500	3.5	850	
	600			
	700			
	800			
	900			
	1000			
	1100			
	1200			
Case 2	900	3.5	650	Fixed 7.0
			750	
			850	
			950	
			1050	
Case 3	900	3.5	850	
		4.5		
		5.5		
		6.5		

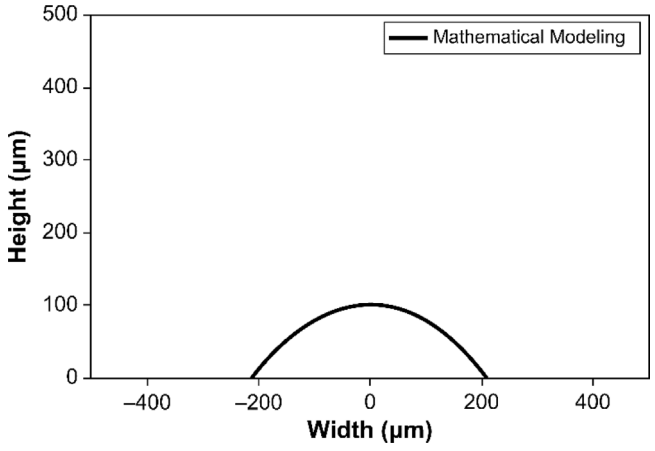

Fig. 3. Single bead geometry of mathematical model.

3 Results and discussion

3.1 Bead shape according to change in laser power

To investigate the effect of laser power, a critical process parameter, on the bead shape, only the laser power was varied while keeping the other process conditions constant. The cross sections of the deposited beads were examined as shown in Figure 4. It was observed that both the width and height of the bead increased with higher laser power. Although some data points may exhibit slight deviations from a linear trend, these deviations do not significantly impact the overall trend. Based on this trend, the coefficient (a) and the constant (c) required in equation (2) to determine the effect of laser power on the bead shape were obtained (Tab. 3).

Previous research conducted by Lee et al. also reported a proportional relationship between laser power and bead width in selective laser melting of SUS316L specimens, which is consistent with our findings [15]. This behavior can be attributed to the relationship between bead shape and laser density, where laser density is directly proportional to power and inversely proportional to beam diameter and head scanning speed. This phenomenon is generally observed when a larger volume of powder is melted due to increased heat input. Therefore, laser power plays a crucial role in determining the width and height of the bead. Figure 5 illustrates the measurements of height and width in the cross-section of the deposited beads in relation to changes in laser power. The analysis of bead cross sections indicates that both the width and height of the bead tend to increase linearly. Thus, by identifying the trends of the experimental width and height information, it is possible to predict the overall shape of the bead

3.2 Bead shape according to changes in scanning speed

To investigate the impact of scanning speed on the bead shape, the process conditions of Case 2 were applied during deposition, and the resulting bead shapes are presented in Figure 6. Analysis of the bead cross section with respect to changes in scanning speed revealed that both the width and height of the bead decreased as the scanning speed increased. This is attributed to the inverse proportionality between scanning speed and energy density. Previous research conducted by Yoo et al. in a study on dissimilar metal welding using Nd:YAG laser deposition also reported that the bead deposition height is inversely proportional to scanning speed, which is consistent with our findings [16].

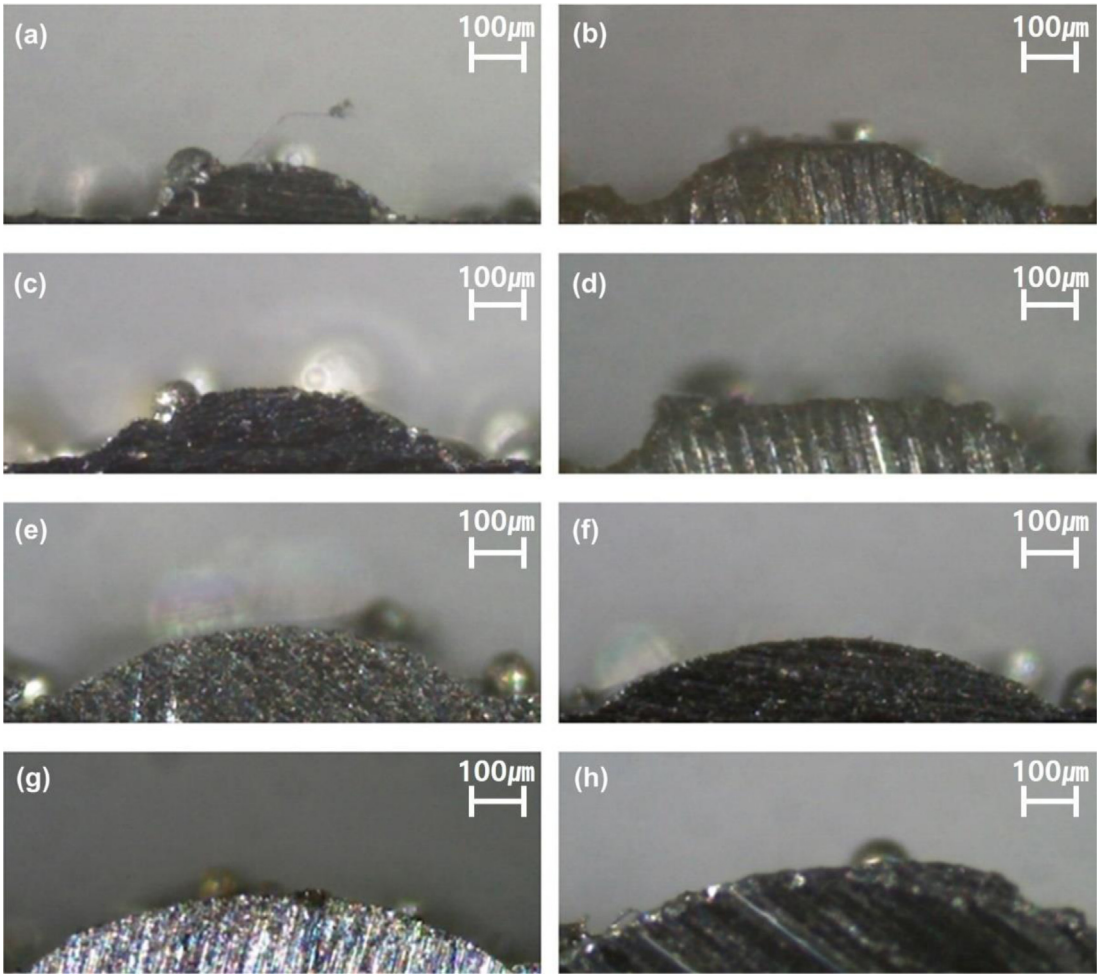

Fig. 4. Bead cross-sectional shape according to laser power; Bead cross section when the laser power is 500W(a), 600W(b), 700W(c), 800W(d), 900W(e), 1000W(f), 1100W(g) and 1200W(h).

Table 3. Correlation between bead shape and laser power (Q).

(A = μm/W)		
	Fitting equation	R-squared
Height (h)	$h = 0.118Q \cdot A + 33.57$	0.9816
Width (w)	$w = 0.644Q \cdot A + 163.81$	0.9663

As the scanning speed increases, the time available for heating the powder decreases, leading to reduced time for sufficient melting and solidification of the powder. As a result, scanning speed plays a crucial role in determining the bead deposition height and heat-affected zone height. Figure 7 illustrates the measurements of height and width in the cross-section of the deposited beads in relation to changes in scanning speed during an actual DED process. From Figures 6 and 7, it can be observed that the measured height and width of the bead tend to decrease linearly. As discussed in Section 3.1, this trend can result in a negative coefficient between scanning speed and bead shape (Tab. 4).

3.3 Bead shape according to changes in powder feed rate

To investigate the impact of powder feed rate on the bead shape, the process conditions of Case 1 were employed during deposition. Figure 8 presents a cross-section of a bead stacked by applying the process conditions of Case 3. It was observed that the height of the bead increased with an increase in the powder feed rate. This can be attributed to the fixed diameter and power of the laser irradiated to the powder, and the adequate melting of the powder. Previous research conducted by Seo et al. in a study on bead characteristics during laser melting deposition found that low powder feed rates may result in excessive heat input, potentially degrading the mechanical properties, while high powder feed rates may lead to insufficient powder melting [17]. Therefore, it is crucial to select an optimal powder feed rate, which ensures sufficient melting of the powder through adequate powder supply. Consequently, the powder feed rate plays a critical role in determining the bead width and the melt pool formation. Figure 9 displays the measurements of height and width in the cross-section of the deposited beads in relation to changes in powder feed rate based on an actual DED

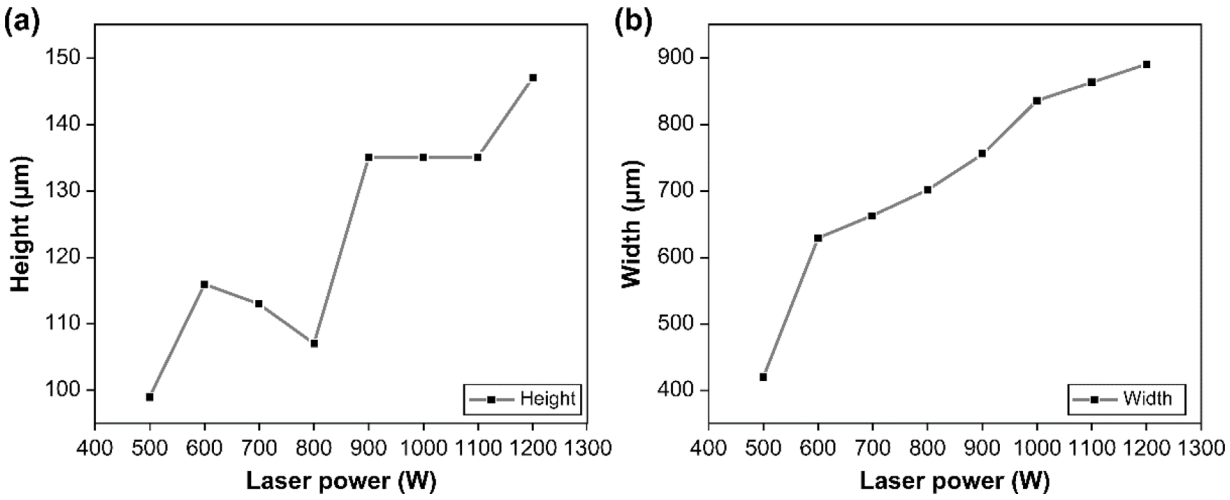

Fig. 5. Effects laser power on bead; (a) height, (b) width.

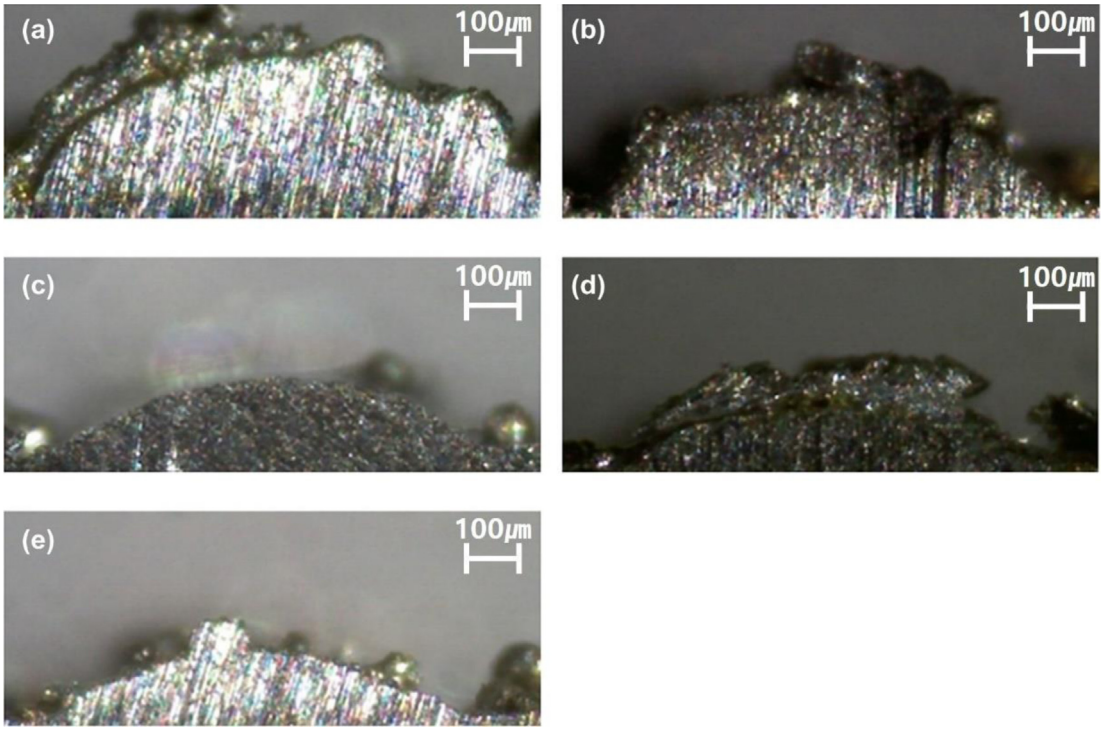

Fig. 6. Bead cross-sectional shape according to scanning speed; Bead cross section when the scanning speed is 650 mm/min(a), 750 mm/min(b), 850 mm/min(c), 950 mm/min(d) and 1050 mm/min(e).

process. From Figures 8 and 9, it is evident that the bead width tends to increase linearly with the powder feed rate. Therefore, the coefficient between the powder feed rate and bead shape is also positive (Tab. 5).

4 Comparison of empirical formulations with real beads

4.1 Empirical formulations according to changes in laser power

Equation (3) presents an empirical formulation that applies the coefficients and constants derived from equation (1) to model the relationship between laser power and bead shape. Figure 10 compares the predicted bead shapes using the empirical formulations with the real deposited beads under varying laser power conditions. As mentioned previously, an increase in laser power results in a higher heat input to the powder, causing the bead width and height to increase as more powder is melted. This is evident in the mathematical prediction model, which shows an increase in width and height with higher laser powers, when compared to the actual bead shapes. To quantify this effect, the cross-sectional area was measured, and the results are depicted in Figure 11. A comparison between

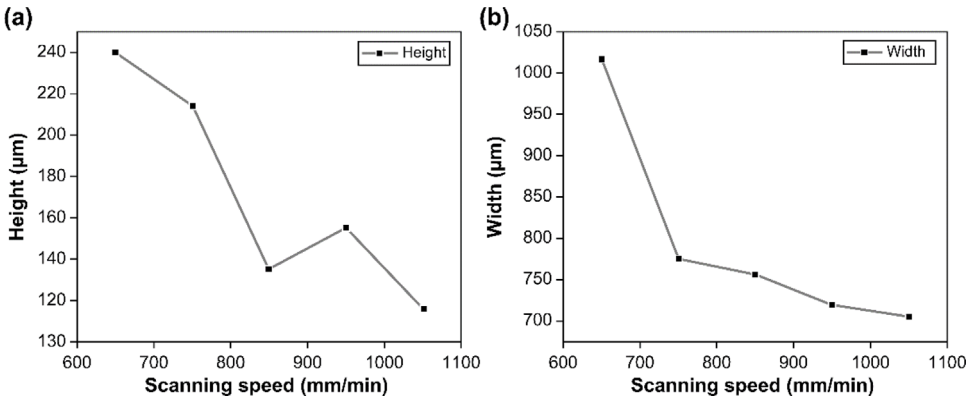

Fig. 7. Effects scanning speed on bead; (a) height, (b) width.

Table 4. Correlation between bead shape and scanning speed (v).

($B = \mu m \cdot min/mm$)		
	Fitting equation	R-squared
Height (h)	$h = -0.210v \cdot B + 335.50$	0.7670
Width (w)	$w = -0.235v \cdot B + 969.25$	0.4914

the empirical formulation area and the actual bead shape revealed a difference ranging from 0.0002 mm^2 to 0.0097 mm^2. This difference can be attributed to distortions and curvatures in the actual deposited bead, which may deviate from a perfect semicircle. For laser powers of 500 and 1000 W, the areas were nearly identical, and for powers of 600 and 700 W, the difference in area was sometimes large. Nevertheless, the maximum error between the areas of the empirical formulation and the actual bead is 0.0097 mm^2, which is negligible in the context of the total bead area. Hence, this discrepancy is not expected to have a significant impact on the comparison between the actual deposited beads and the empirical formulations.

$$y = -\frac{4(0.644Q + 163.81)}{(0.118Q + 33.57)^2}x^2 + 0.644Q + 163.81, (y \geq 0). \quad (3)$$

4.2 Empirical formulations according to changes in scanning speed

Equation (4) presents an empirical formulation that applies the derived coefficients and constant to model the relationship between scanning speed and bead shape, as obtained from equation (1). Figure 12 compares the predicted bead shapes using the empirical formulations with the real deposited beads under varying scanning speed conditions. As scanning speed is inversely proportional to the powder feed rate and energy supplied per unit time, the bead width and height tend to decrease with higher scanning speeds. This trend is also observed in the empirical formulations. Figure 13 shows a comparison between the empirical formulation area and the actual bead shape. The maximum difference in area was found to be 0.0071 mm^2. This discrepancy may arise due to the presence of partial melting powder around the bead shape when the cross-section of the deposited bead is cut to measure the area. Since the scanning speed is not optimized with respect to other process conditions, the material may not completely melt, resulting in the formation of partial melting powder around the bead shape. Models (b) and (c) in Figure 13 showed minimal presence of partial melting powder, and thus, the actual deposited area closely matched the empirical formulations. On the other hand, models (a), (d), and (e) exhibited partial melting powder, leading to discrepancies between the areas of the bead derived from the empirical formulations and the actual deposited bead.

$$y = -\frac{4(-0.21v + 335.5)}{(-0.235v + 969.25)^2}x^2 - 0.21v + 335.5, (y \geq 0). \quad (4)$$

4.3 Empirical formulations according to changes in powder feed rate

Equation (5) presents an empirical formulation that applies the derived coefficients and constant to model the relationship between powder feed rate and bead shape, as obtained from equation (1). Figure 14 compares the predicted bead shapes using the empirical formulations with the real deposited beads under varying powder feed rate conditions. As shown in Figure 14, as the powder feed rate increases, the bead height tends to increase. This can be attributed to the excessive metal powder being supplied while the laser power remains constant, resulting in decreased absorption of the heat source and reduced energy absorbed by the substrate, making it difficult to create a melt pool [18]. If the powder feed rate is too high, the metal powder may not be sufficiently melted, highlighting the importance of determining the optimal powder feed rate for deposition.

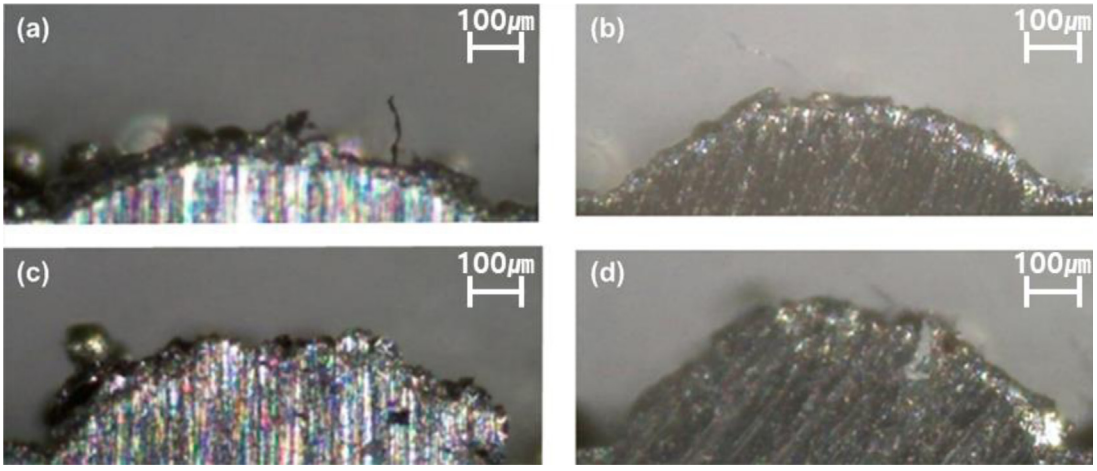

Fig. 8. Bead cross-sectional shape according to powder feed rate; Bead cross section when the powder feed rate is 3.5 g/min(a), 4.5 g/min(b), 5.5 g/min(c) and 6.5 g/min(d).

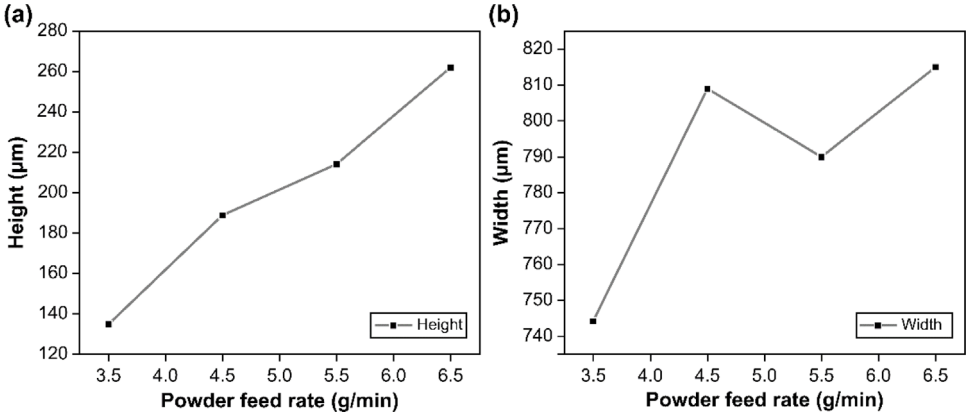

Fig. 9. Effects powder feed rate on bead; (a) height, (b) width.

Table 5. Correlation between bead shape and powder feed rate (m).

	($C = \mu m \cdot min/g$)	
	Fitting equation	R-squared
Height (h)	$h = 31m \cdot C + 5.5$	0.9515
Width (w)	$w = 7.5m \cdot C + 722.5$	0.7627

Figure 15 demonstrates that when the powder feed rate is set at 4.5 g/min, the areas of the shape derived from the empirical formulation and the actual shape are nearly identical. Thus, a powder feed rate of 4.5 g/min is estimated to be an optimal process parameter for bonding the metal powder and substrate. Furthermore, as shown in Figure 14c, when the powder feed rate increases, the bead height also increases, but the heat input decreases, potentially leading to reduced accuracy in the bead shape due to partial melting powder caused by unmelted metal powder.

$$y = -\frac{4(7.5m + 722.5)}{(31m + 5.5)^2}x^2 + 31m + 5.5, (y \geq 0). \quad (5)$$

5 Empirical bead volume

Figure 16 showcases a successfully created volume model of a single bead using the bead cross-sectional profile and deposited length value. The equation for deriving the empirical formulation of the bead cross-section is multiplied by the length to formulate equation (6). Additionally, by integrating the cross-sectional area calculated using the width and height of the deposited bead and multiplying it by the deposited length, the volume of a single bead can be obtained. Table 6 presents the volumes calculated using the cross-sections derived in this study, which can be utilized for further analyses, such as additive manufacturing processes or computer-aided engineering, to determine

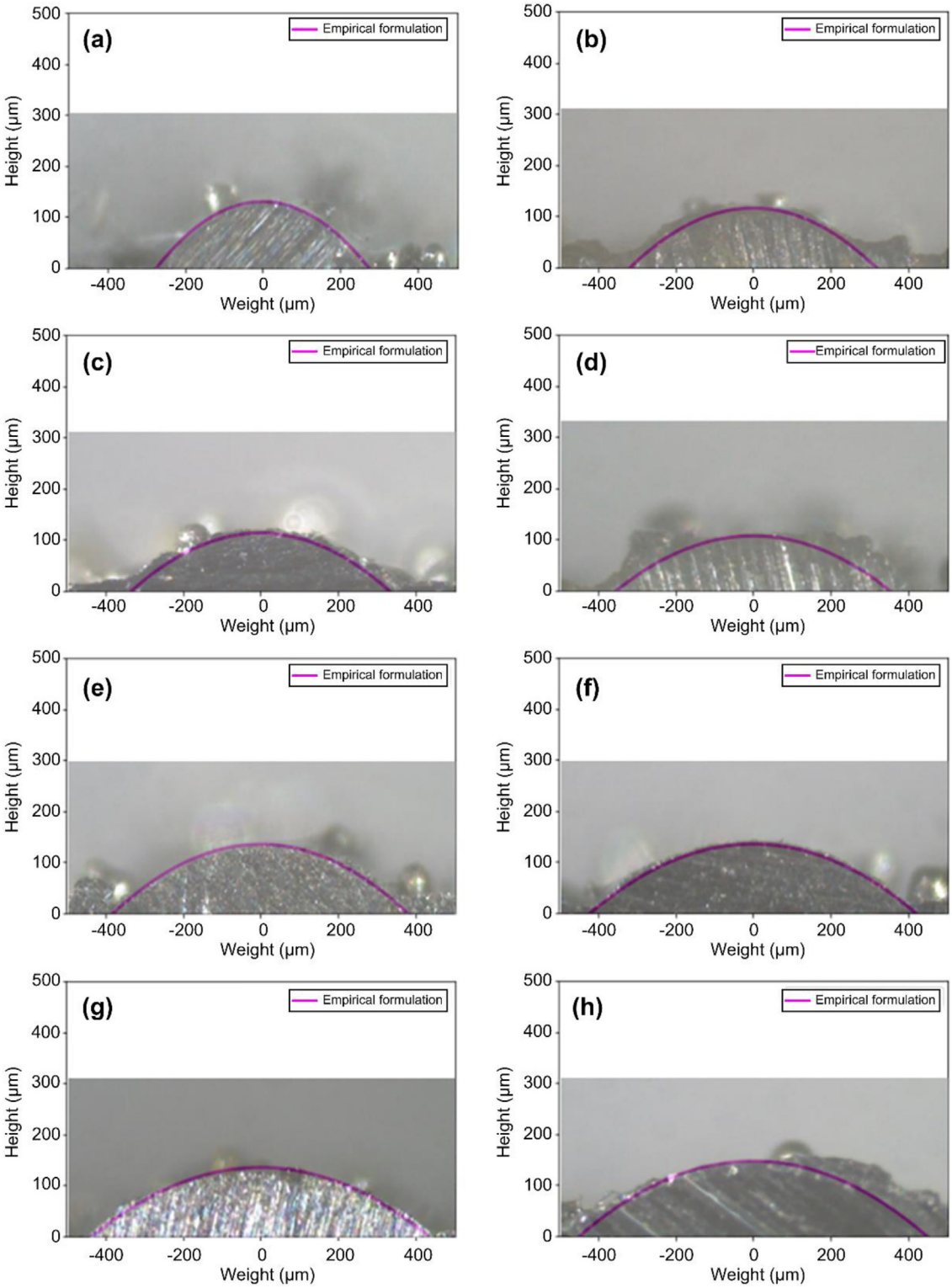

Fig. 10. Comparison with the bead and empirical formulations of laser power; empirical formulation derived when the laser power is 500W(a), 600W(b), 700W(c), 800W(d), 900W(e), 1000W(f), 1100W(g) and 1200W(h).

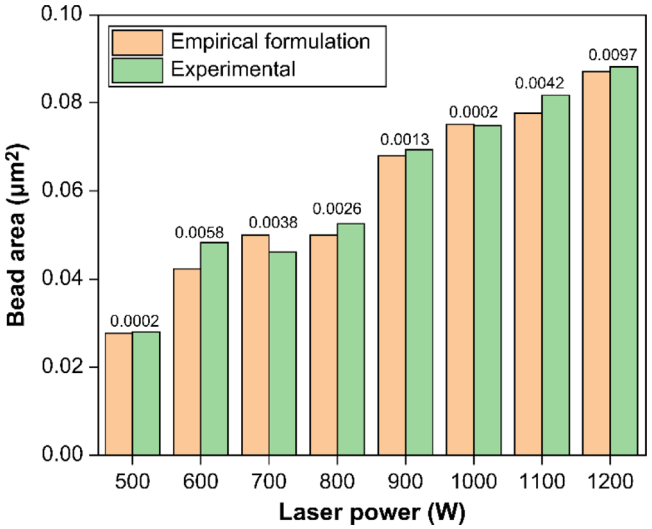

Fig. 11. Comparison of empirical formulation and experimental area of bead cross section according to laser power.

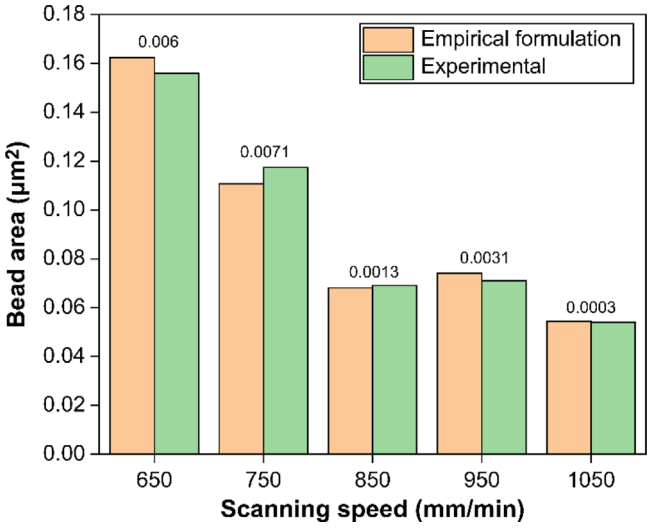

Fig. 13. Comparison of empirical formulation and experimental area of bead cross section according to scanning speed.

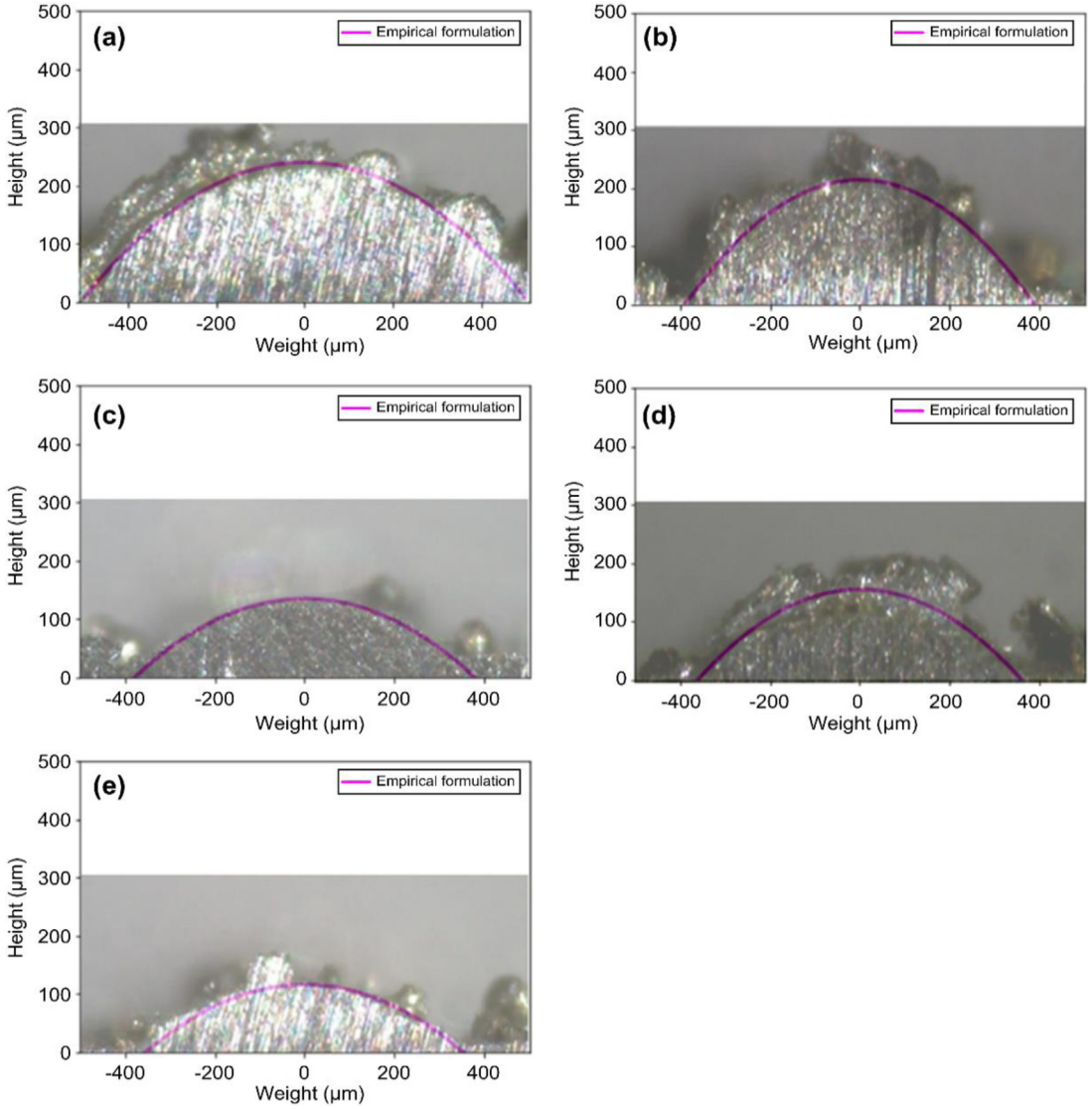

Fig. 12. Comparison with the bead and empirical formulations of scanning speed. Empirical formulation derived when the scanning speed is 650 mm/min(a), 750 mm/min(b), 850 mm/min(c), 950 mm/min(d) and 1050 mm/min(e).

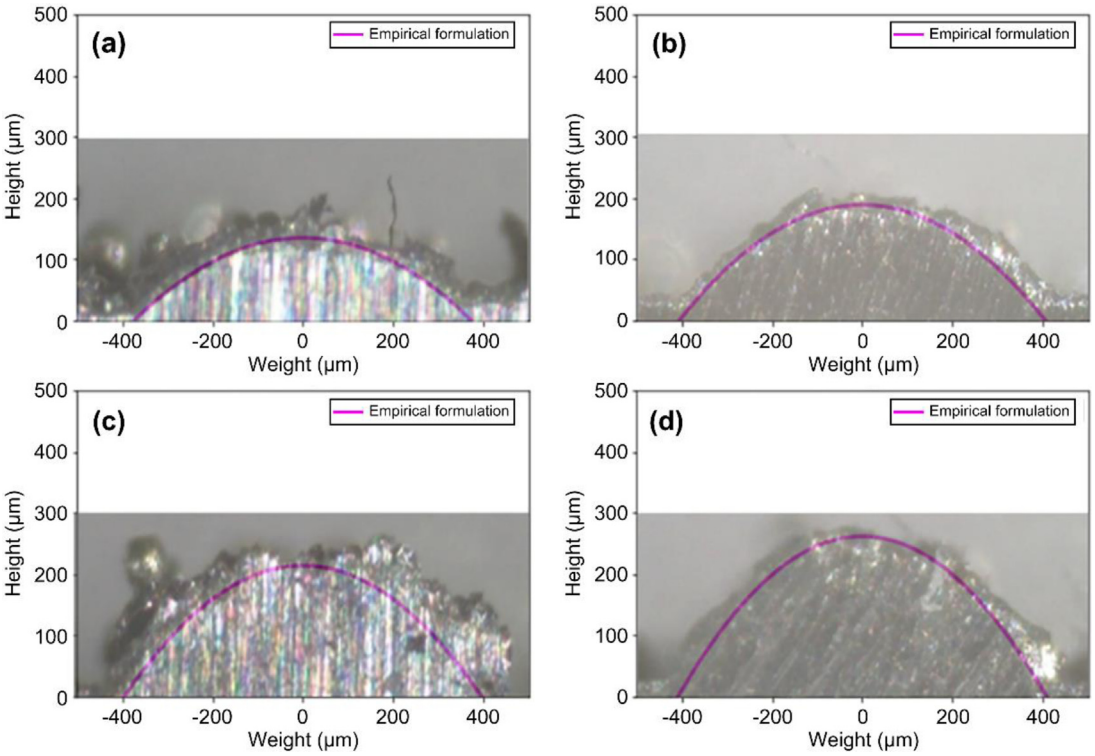

Fig. 14. Comparison with the bead and empirical formulations of powder feed rate. Empirical formulation derived when the powder feed rate is 3.5 g/min(a), 4.5 g/min(b), 5.5 g/min(c) and 6.5 g/min(d).

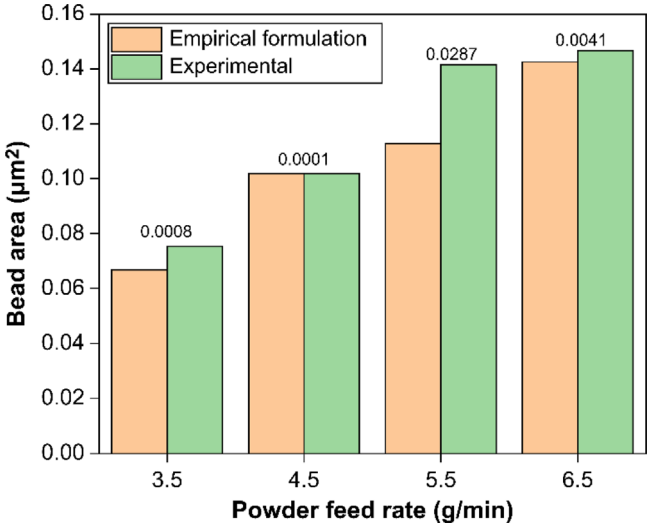

Fig. 15. Comparison of empirical formulation and experimental area of bead cross section according to powder feed rate.

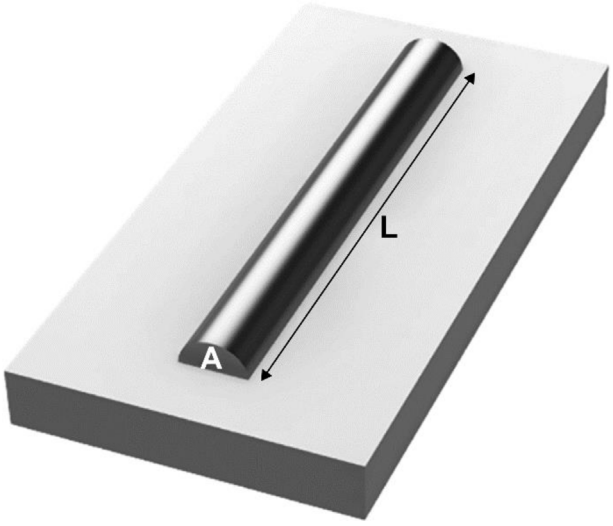

Fig. 16. Parameter of single bead volume.

the volume of a single deposited bead.

$$\left\{ \int_{-\frac{w}{2}}^{\frac{w}{2}} (ax^2 + c)dx \right\} \times l. \tag{6}$$

6 Conclusions

In this study, the impact of different process parameters on the formation of the deposited bead using the DED process with SUS316 powder was investigated. The results showed that the bead width and height changed in response to the

Table 6. Volumes of experimental and empirical formulation.

Experiment	Variable	Experimental volume	Empirical formulation volume
Case 1	500	0.696	0.691
	600	1.201	1.056
	700	1.152	1.247
	800	1.316	1.252
	900	1.734	1.701
	1000	1.873	1.879
	1100	2.047	1.942
	1200	2.207	2.183
Case 2	650	3.913	4.064
	750	2.942	2.764
	950	1.78	1.857
	1050	1.355	1.363
Case 3	3.5	1.885	1.674
	4.5	2.545	2.548
	5.5	3.536	2.818
	6.5	3.66	3.559

process parameters. An empirical equation to express the bead shape based on information on the bead width and height was successfully formulated. The following conclusions were drawn:

– The width and height of the bead cross-section changed linearly with the laser power, scanning speed, and powder feed rate, which were highly correlated with energy density and heat input. Specifically, the laser power and powder feed rate were directly proportional to the bead width and height, while the scanning speed was inversely proportional.
– The bead shape was expressed using an empirical formulation based on information on the bead width and height, and the comparison between the cross-sectional areas of beads formed by the empirical formulation and those of actual deposited beads showed similar results.
– We were able to calculate the volume of a single bead by utilizing the cross-sectional information and deposited length value of the bead.

In this study, we have formulated equations to predict the cross-sectional shape and volume of a single bead in the metal additive manufacturing process. These equations serve as fundamental data for creating analytical models. In the DED process, bead size is determined by multiple interacting variables, rather than a single factor. Our research conclusively demonstrates how bead size and shape vary with different process conditions, and we have successfully predicted these variations using mathematical models. This method allows for the precise prediction of bead dimensions or the necessary process conditions to achieve specific bead sizes, thereby reducing the reliance on extensive empirical experimentation. This capability can significantly cut down on the time and costs associated with experimental setups. Further research is necessary to expand these findings to include analyses of heat transfer and stress changes in multi-bead and multi-layer processes. By addressing this critical industrial challenge, our study simplifies and enhances control over the production process, facilitating substantial time and cost savings through detailed analysis [19,20].

Funding

This results was supported by "Regional Innovation Strategy (RIS)" through the National Research Foundation of Korea (NRF) funded by the Ministry of Education(MOE) (2021RIS-002) and was co-supported by research funds from Gwangju University in 2025. The funding agencies had no role in study design; in the collection, analysis and interpretation of data; in the writing of the report; and in the decision to submit the article for publication.

Conflicts of interest

The author declares no conflicts of interest relevant to this study.

Data availability statement

The data supporting the findings of this study are available from the corresponding author upon reasonable request.

Author contribution statement

I am the sole author of this paper.

References

[1] Q. Ming, L.C. Lima, Z.D. Chen, Laser cladding of nickel-based hard facing alloys, Surf. Coat. Technol. **106**, 174–182 (1998)

[2] C. Lalas, K. Tsirbas, K. Salonitis, G. Chryssolouris, An analytical model of the laser clad geometry, Int. J. Adv. Manuf. Technol. **32**, 34–41 (2007)

[3] Y. Sun, M. Hao, Statistical analysis and optimization of process parameters in Ti6Al4V laser cladding using Nd:YAG laser, Opt. Lasers Eng. **50**, 985–995 (2012)

[4] U. de Oliveira, V. Ocelík, J.T.M. De Hosson, Analysis of coaxial laser cladding processing conditions, Surf. Coat. Technol. **197**, 127–136 (2005)

[5] J.H. Hwang, S.S. Shin, J.H. Lee, S.W. Kim, H.D. Kim, A study on Surface and cross-section properties depending on the process parameters of laser depositions with metal powders (SUS316L and IN718), Weld. Joining, **35**, 28–34 (2017)

[6] S.S. Shin, S.M. Kwon, C.Y. Kim, J.H. Lee, J.H. Hwang, H.D. Kim, Optimization of direct energy deposition of 304L stainless steel through laser process parameters, Weld. Joining, **39**, 182–188 (2021)

[7] K.H. Han, J.G. Kim, C.H. Kim, J.H. Kim, S.H. Nam, C.J. Jun, Effects of GMA welding conditions on the bead shape of hard facing overlay welding, J. KWJS, **25**, 58–63 (2017)

[8] G. Bi, A. Gasser, K. Wissenbach, A. Drenker, R. Poprawe, Characterization of the process control for the direct laser metallic powder deposition, surface and coatings technology, J. Mech. Sci. Technol. **201**, 2676–2683 (2006)

[9] I.S. Kim, M.H. Park, A review on optimizations of welding parameters in GMA welding process, Korean Weld. Join. Soc. **36**, 65–75 (2018)

[10] J.S. Kim, I.J. Kim, Y.G. Kim, Optimization of weld pitch on overlay welding using mathematical method, Int. J. Precis. Eng. Manuf. **15**, 1117–1124 (2014)

[11] V. Dey, D.K. Pratihar, G.L. Datta, M.N. Jha, T.K. Saha, A.V. Bapat, Optimization of bead geometry in electron beam welding using a genetic algorithm, J. Mater. Process. Technol. **209**, 1151–1157 (2009)

[12] K. Siva, N. Murugan, V. Raghupathy, Modelling, analysis and optimization of weld bead parameters of nickel based overlay deposited by plasma transferred arc surfacing, Arch. Comp. Mater. Sci. Surf. Eng. **1**, 174–182 (2009)

[13] H. El Cheikh, B. Courant, S. Branchu, J.-Y. Hascoët, R. Guillén, Analysis and prediction of single laser tracks geometrical characteristics in coaxial laser cladding process, Opt. Lasers Eng. **50**, 413–422 (2012)

[14] J.P. Paulo Davim, C. Oliveira, A. Cardoso, Predicting the geometric form of clad in laser cladding by powder using multiple regression analysis (MRA), Mater. Des. **29**, 554–557 (2008)

[15] D.W. Lee, W.S. Kim, J.H. Sung, C. Kim, H.J. Lee, Impact of energy density and bead overlap ratio of a SUS316L specimen fabricated using selective laser melting on mechanical characteristics, J. Korean Soc. Manuf. Process Eng. **20**, 42–51 (2021)

[16] Y.T. Yoo, H.J. Shin, D.G. Ahn, I. Kie Gon, B.H. Shin, Dissimilar metal welding of medium carbon steel and austenitic stainless steel utilize CW Nd:YAG Laser, J. Korean Soc. Precis. Eng. **23**, 47–55 (2006)

[17] J.Y. Seo, H.S. Yoon, K.Y. Lee, D.S. Shim, Study on effects of direct laser melting process parameters on deposition characteristics of AlSi12 powders, Trans. Mater. Process. **27**, 314–322 (2018)

[18] E.M. Lee, G.Y. shin, H.S. Yoon, D.S. Shim, Study of the effects of process parameters on deposited single track of M4 powder based direct energy deposition, J. Mech. Sci. Technol. **31**, 3411–3418 (2017)

[19] H. Ijaz, M. Danish, M. Asad, S. Rubaiee, A three-dimensional finite element-approach to investigate the optimum cutting parameters in machining AA2024, Mechanics & Industry, **21**, 615 (2020)

[20] T. Daniel, F. Casenave, N. Akkari, D. Ryckelynck, C. Rey, Uncertainty quantification for industrial numerical simulation using dictionaries of reduced order models, Mechanics & Industry, **23**, (2022)

Cite this article as: G.-Y. Baek, Empirical formulation for bead shape prediction in direct energy deposition, Mechanics & Industry 26, 7 (2025), https://doi.org/10.1051/meca/2024037